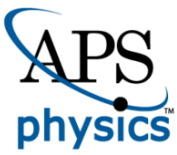

Impenetrable SU(N) fermions in one-dimensional lattices

Yicheng Zhang, Lev Vidmar, and Marcos Rigol

Phys. Rev. A **98**, 042129 — Published 25 October 2018

DOI: 10.1103/PhysRevA.98.042129

Impenetrable SU(N) fermions in one-dimensional lattices

Yicheng Zhang,[1,2] Lev Vidmar,[2] and Marcos Rigol[1]

[1] *Department of Physics, The Pennsylvania State University, University Park, Pennsylvania 16802, USA*
[2] *Department of Theoretical Physics, J. Stefan Institute, Ljubljana, Slovenia*

We study SU(N) fermions in the limit of infinite onsite repulsion between all species. We focus on states in which every pair of consecutive fermions carries a different spin flavor. Since the particle order cannot be changed (because of the infinite onsite repulsion) and contiguous fermions have a different spin flavor, we refer to the corresponding constrained model as a model of distinguishable quantum particles. We introduce an exact numerical method to calculate equilibrium one-body correlations of distinguishable quantum particles based on a mapping onto noninteracting spinless fermions. In contrast to most many-body systems in one dimension, which usually exhibit either power-law or exponential decay of off-diagonal one-body correlations with distance, distinguishable quantum particles exhibit a Gaussian decay of one-body correlations in the ground state, while finite temperature correlations are well described by a stretched exponential decay.

I. INTRODUCTION

Low dimensionality can give rise to fascinating phenomena. A striking one, which occurs when interacting spinful particles are confined in one dimension, is the so-called spin-charge separation [1, 2]. This phenomenon has been studied experimentally in a wide range of systems including quasi-one-dimensional compounds [3–6], grain boundaries in semiconductors [7], and ultracold atoms in optical lattices [8, 9]. Theoretically, a cornerstone in the understanding of the low-energy properties of one-dimensional (1D) systems is provided by the Luttinger liquid theory [10–13], which, among others, naturally describes spin-charge separation and predicts the existence of power-law correlations in gapless ground states.

Recent impetus to the study of many-body quantum systems in one dimension has been provided by experimental advances with ultracold quantum gases in optical lattices [13, 14]. In optical lattices, it is possible to realize very strong correlations in one dimension so that, e.g., bosons with contact interactions behave as impenetrable particles and "fermionize" [15–18]. Another remarkable possibility opened by experiments with ultracold gases is the use of fermionic alkaline earth atoms to realize SU(N) models [19–25] (see Ref. [26] for a review). The latter possibility has motivated theoretical studies on spin chains and quantum gases beyond the more traditionally considered SU(2) case [27–33].

Both, the realization of SU(N) models as well as the achievement of regimes in one dimension in which particles become "impenetrable" are important motivations for this work. In the limit of infinite contact repulsion between spinful particles, the spin and charge degrees of freedom decouple at all energies. This can be used to construct many-body wavefunctions [34]. Physical properties of spinful impenetrable particles have been studied within different models, ranging from fermionic models [33, 35–44] to classical systems [45].

Here we study impenetrable SU(N) fermions, which can be thought of as the limit of infinite onsite repulsion between all spin flavors in a generalized one-dimensional SU(N) Hubbard model. In such a limit, sectors of the Hamiltonian with different spin configurations are degenerate. Such independent sectors are in principle accessible in experiments with ultracold atoms in optical lattices via spin-resolved manipulation techniques to imprint desirable spin patterns [46]. In this study, we focus on sectors in which contiguous fermions have different spin flavors. For eigenstates of the Hamiltonian in those sectors, we introduce an exact numerical method to calculate one-body correlations via a mapping onto noninteracting spinless fermions. This method is used to study properties of ground states with special spin flavor patterns, namely, with generalized Neel order. Figures 1(a)–1(c) display examples of many-particle configurations of interest in this work, while Fig. 1(d) displays an example which does not satisfy the requirement of contiguous fermions having different spin flavors.

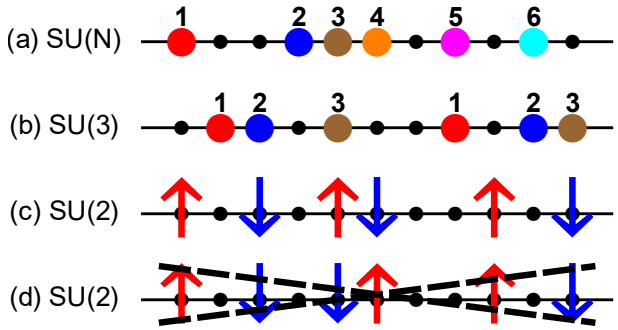

FIG. 1. Particle configurations of SU(N) fermions on a chain with $N_p = 6$ particles. (a)–(c) Configurations in which every pair of consecutive particles carries a distinct spin flavor, and in which there is an identical spin flavor pattern that we call generalized Neel order. Configurations (a)–(c) can be described by the model of distinguishable quantum particles introduced in this work. (d) A configuration that cannot be described by the model of distinguishable quantum particles.

Since particle exchange is forbidden in the limit of in-

finite onsite repulsion between all spin flavors, and contiguous fermions have a different spin flavor in the many-particle configurations of interest here, we refer to the corresponding constrained model as a model of *distinguishable* quantum particles. Note that the ground state and finite temperature states (also studied in this work) of distinguishable quantum particles are not the ground state and finite temperature states of the SU(N) Hubbard model in the limit of infinite onsite repulsion. The latter involve states with exponentially many spin configurations. SU(N) fermions with infinite onsite repulsion become distinguishable only if one constrains the system to be in a sector with a specific spin configuration in which contiguous fermions have a different spin flavor.

Another motivation for this study is the fact that our constrained SU(N) model exhibits fundamentally different off-diagonal one-body correlations when compared to unconstrained models. For the latter, the exact Bethe Ansatz solution for 1D SU(2) Hubbard model was obtained by Lieb and Wu [47], and simplified by Ogata and Shiba in the limit of infinite repulsion [34]. Here, we show that one-body correlations in the ground state of distinguishable quantum particles exhibit a Gaussian decay with distance, in contrast to the power law decay of the unconstrained SU(2) case [38, 48]. At finite temperature, one-body correlations are shown to be well described by a stretched exponential decay, with an exponent that transitions (with increasing temperature) between the Gaussian decay at zero temperature and an exponential decay at high temperature.

The presentation is organized as follows. In Sec. II, we introduce the constrained SU(N) model for distinguishable quantum particles and the methodology developed to evaluate its one-body correlations. Numerical results for such correlations are presented in Sec. III for the ground state, and in Sec. IV for finite temperatures. A summary of the results is presented in Sec. V.

II. SETUP AND FORMALISM

We start with a generalized one-dimensional Hubbard model for SU(N) fermions with infinite onsite repulsion. The model Hamiltonian for a chain with open boundaries can be written as

$$\hat{H}_N = -J \sum_{l=1}^{L-1} \sum_{\sigma=1}^{N} \left[\hat{f}_l^{(\sigma)\dagger} \hat{f}_{l+1}^{(\sigma)} + \hat{f}_{l+1}^{(\sigma)\dagger} \hat{f}_l^{(\sigma)} \right] , \qquad (1)$$

where L is the number of lattice sites, σ denotes spin flavor (in our notation, $\sigma \in \{1, ..., N\}$), and $\hat{f}_l^{(\sigma)\dagger}$ ($\hat{f}_l^{(\sigma)}$) is the creation (annihilation) operator for a fermion with spin σ at site l. Infinite onsite repulsion is enforced by the constraints $\hat{f}_l^{(\sigma)\dagger} \hat{f}_l^{\dagger(\sigma')} = \hat{f}_l^{(\sigma)} \hat{f}_l^{(\sigma')} = 0$. The hopping amplitude J and the lattice spacing are set to unity.

The Hamiltonian $\hat{H}_N$ in Eq. (1) commutes with the total particle number operator for any given spin flavor $\hat{N}_p^{(\sigma)} = \sum_{l=1}^{L} \hat{f}_l^{(\sigma)\dagger} \hat{f}_l^{(\sigma)}$ (the total number of particles with any given spin flavor is conserved), and hence with the total number of particle operator $\hat{N}_p = \sum_{\sigma=1}^{N} \hat{N}_p^{(\sigma)}$. Moreover, as a consequence of infinite onsite repulsion, $\hat{H}_N$ also preserves any configuration of spin flavors. Hence, for a given total particle number N_p, the Hamiltonian consists of degenerate sectors, where every block is associated with the spin configuration $\underline{\sigma} = \{\sigma_1, ..., \sigma_{N_p}\}$ ($\sigma_j \in \{1, ..., N\}$). Eigenstates within a block are linear superpositions of base kets of the form

$$|\varphi_{\underline{x},\underline{\sigma}}\rangle = \prod_{j=1}^{N_p} \hat{f}_{x_j}^{(\sigma_j)\dagger} |\emptyset\rangle \, , \qquad (2)$$

where $\underline{x} = \{x_1, ..., x_{N_p}\}$ denotes the set of occupied sites, $x_j \in \{1, ..., L\}$, and $x_1 < x_2 < ... < x_{N_p}$.

We study the impenetrable SU(N) model, with Hamiltonian $\hat{H}_N$ in Eq. (1), within a sector with a given spin configuration $\underline{\sigma}$. This is a model of relevance to experiments with ultracold quantum gases in optical lattices in which such spin configurations can be constructed using, e.g., spin-resolved manipulation techniques (which can be applied on simple product states [46]) followed by adiabatic or quasi-adiabatic transformations.

A. Model of distinguishable quantum particles

The next essential constraint imposed on the states we study, in addition to being for impenetrable SU(N) fermions within a single spin configuration $\underline{\sigma}$ sector, is that we require the spin configuration $\underline{\sigma}$ to have every pair of consecutive fermions carry distinct spin flavors

$$\underline{\sigma} = \{\{\sigma_j\} \, ; \, j = 1, ..., N_p \, ; \, \sigma_j \neq \sigma_{j+1} \, \forall \, j < N_p\} \, . \qquad (3)$$

This implies that particle exchanges are forbidden. We call the constrained SU(N) model, in which the spin configuration obeys the condition in Eq. (3), a model of distinguishable quantum particles (DQPs).

Of particular interest to us will be the DQP model in which the spin configuration forms a periodic structure, which we call a generalized Neel order. Those configurations have:

$$\underline{\sigma} = \{\{\sigma_j\} \, ; \, j = 1, ..., N_p \, ; \, \sigma_j = [(j-1) \bmod N] + 1\} \, , \qquad (4)$$

Examples of such configurations are schematically shown in Fig. 1. Note that, in the SU(2) case, the spin configurations that obey Eq. (3) also obey Eq. (4).

At this point it is important to stress that while we have arrived to the model of DQPs thinking about experiments with impenetrable SU(N) fermions, the approach we develop in what follows and the results we obtain apply equally to systems of spinful impenetrable bosons. Under the constraints of our construction, the original particle statistics plays no role.

B. Spin-charge decoupling

For a given spin configuration $\underline{\sigma}$, charge degrees of freedom of the constrained SU(N) model can be described by the spinless fermion Hamiltonian

$$\hat{H}_{\rm SF} = -\sum_{l=1}^{L-1} (\hat{c}_l^\dagger \hat{c}_{l+1} + \hat{c}_{l+1}^\dagger \hat{c}_l)\,, \tag{5}$$

where $\hat{c}_l^\dagger$ ($\hat{c}_l$) is the spinless fermion creation (annihilation) operator in lattice site l. The challenge that remains is to take into account the spin degrees of freedom to compute spin-resolved off-diagonal correlation functions.

Our solution to this challenge is based on the following ansatz within the model of DQPs for the spin-resolved one-body correlations $\hat{C}_l^\sigma(x) = \hat{f}_{l+x}^{(\sigma)\dagger} \hat{f}_l^{(\sigma)}$, between sites l and $l+x$,

$$C_l^\sigma(x) = \langle\Psi|\hat{f}_{l+x}^{(\sigma)\dagger} \hat{f}_l^{(\sigma)}|\Psi\rangle = \langle\Psi_{\rm SF}|\hat{c}_{l+x}^\dagger \hat{c}_l\, \hat{\mathcal{P}}_{l,x}^{(\sigma)}|\Psi_{\rm SF}\rangle\,, \tag{6}$$

where $|\Psi\rangle$ and $|\Psi_{\rm SF}\rangle$ are eigenstates (we focus on the ground state later) of $\hat{H}_N$ (in the sector with the desired spin order) and $\hat{H}_{\rm SF}$, respectively. $\hat{\mathcal{P}}_{l,x}^{(\sigma)}$ is a spin projection operator that acting on $|\Psi_{\rm SF}\rangle$ produces a (polynomially large in the system size) sum of Slater determinants. The final expression in Eq. (6) can be efficiently evaluated in polynomial time using properties of Slater determinants, as done for hard-core bosons in Refs. [49, 50].

C. Spin projection operator

We construct the projection operator $\hat{\mathcal{P}}_{l,x}^{(\sigma)}$ as a product of two operators

$$\hat{\mathcal{P}}_{l,x}^{(\sigma)} = \hat{\mathcal{M}}_{l,x} \hat{\mathcal{R}}_l^{(\sigma)}\,. \tag{7}$$

The role of the operator $\hat{\mathcal{M}}_{l,x}$ is to prevent an exchange of particles that would result in a change of the spin configuration in the SU(N) model. This operator must annihilate many-body states in which any of the lattice sites $j \in \{l+1, ..., l+x-1\}$ is occupied. This is achieved by defining

$$\hat{\mathcal{M}}_{l,x} = \prod_{j=l+1}^{l+x-1} \left(1 - \hat{c}_j^\dagger \hat{c}_j\right)\,. \tag{8}$$

On the other hand, the role of the operator $\hat{\mathcal{R}}_l^{(\sigma)}$ is to target spin flavor σ at site l. Let us first focus on spin configurations with a generalized Neel order, Eq. (4). (We consider arbitrary spin configurations within the DQP model right after.) We define $\hat{\mathcal{R}}_l^{(\sigma)}(N)$ as

$$\hat{\mathcal{R}}_l^{(\sigma)}(N) = \frac{1}{N} \sum_{k=0}^{N-1} e^{-\frac{2\pi i}{N}\sigma k} \exp\left[\frac{2\pi i}{N} k \sum_{j=1}^{l} \hat{c}_j^\dagger \hat{c}_j\right]\,. \tag{9}$$

This operator, which involves counting the particles in sites 1 through l, ensures that the number of particles between sites 1 and l is the appropriate one for the given spin flavor σ to occur at site l. To prove it, one can express the wavefunction $|\Psi_{\rm SF}\rangle$ as a sum of many-body states $|\phi_a^l\rangle$, where each $|\phi_a^l\rangle$ is a linear superposition of base kets that share a common property, namely, that the total number of particles in sites 1 through l is a.

We focus on the case in which $L - l \geq N_p - 1$ (similar formulae can be derived for $L - l < N_p - 1$). The decomposition in terms of $|\phi_a^l\rangle$ implies that

$$\sum_{j=1}^{l} \hat{c}_j^\dagger \hat{c}_j |\Psi_{\rm SF}\rangle = \sum_{m=1}^{m_{\rm max}} \sum_{\sigma'=1}^{\sigma_{\rm max}(m)} [(m-1)N + \sigma'] |\phi_{(m-1)N+\sigma'}^l\rangle, \tag{10}$$

where $m_{\rm max}$ and $\sigma_{\rm max}(m)$ are such that all the possible particle numbers in sites 1 through l are included. If $l \leq N_p$, then $m_{\rm max} = \lceil l/N \rceil$, $\sigma_{\rm max}(m < m_{\rm max}) = N$, and $\sigma_{\rm max}(m_{\rm max}) = l - (m_{\rm max} - 1)N$. On the other hand, if $l > N_p$, then $\sigma_{\rm max}(m) = N$ and $m_{\rm max} = N_p/N$. We assume that N_p/N is integer.

Using Eq. (10), the projector $\hat{\mathcal{R}}_l^{(\sigma)}(N)$ acting on $|\Psi_{\rm SF}\rangle$ yields

$$\begin{aligned} &\hat{\mathcal{R}}_l^{(\sigma)}(N)|\Psi_{\rm SF}\rangle \\ &= \sum_{m=1}^{m_{\rm max}} \sum_{\sigma'=1}^{\sigma_{\rm max}(m)} \frac{1}{N} \sum_{k=0}^{N-1} e^{-\frac{2\pi i}{N}(\sigma-\sigma')k} |\phi_{(m-1)N+\sigma'}^l\rangle \\ &= \sum_{m=1}^{m_{\rm max}} \sum_{\sigma'=1}^{\sigma_{\rm max}(m)} \delta_{\sigma,\sigma'} |\phi_{(m-1)N+\sigma'}^l\rangle = \sum_{m=1}^{m'_{\rm max}} |\phi_{(m-1)N+\sigma}^l\rangle\,, \end{aligned} \tag{11}$$

where $m'_{\rm max} = m_{\rm max}$ if $\sigma_{\rm max}(m_{\rm max}) \geq \sigma$, and $m'_{\rm max} = m_{\rm max} - 1$ otherwise. We then see that $\hat{\mathcal{R}}_l^{(\sigma)}(N)|\Psi_{\rm SF}\rangle$ results in states with the desired numbers of particles between sites 1 and l, so that if there is a particle at site l it must have flavor σ.

Equation (9) can be rewritten in a simple form for the SU(2) case, where the spin is either up ($\sigma = 1$) or down ($\sigma = 2$). In this case

$$\hat{\mathcal{R}}_l^{(\sigma)}(2) = \frac{1}{2}\left(1 + (-1)^\sigma \exp\left[i\pi \sum_{j=1}^{l} \hat{c}_j^\dagger \hat{c}_j\right]\right)\,. \tag{12}$$

Another interesting limit is the case in which $N = N_p$ so that every particle carries a distinct spin flavor. As a consequence, every σ can be uniquely assigned to a particle j, resulting in σ_j. Then, the projector $\hat{\mathcal{R}}_l^{(\sigma)}(N_p) = \hat{\mathcal{R}}_l^{(\sigma_j)}(N_p)$ can target any particle $j \in \{1, ..., N_p\}$. We denote one-body correlations in that case as $C_l^{\sigma_j}(x)$. Those correlations can be used to compute $C_l^\sigma(x)$ for any eigenstate of $\hat{H}_N$ in a sector with a desired spin order obeying the condition in Eq. (3):

$$C_l^\sigma(x) = \sum_{\sigma_j = \sigma} C_l^{\sigma_j}(x)\,. \tag{13}$$

Note that the previous expression can also be used for spin configurations exhibiting the generalized Neel order in Eq. (4). However, given the operators defined in Eqs. (7)–(9), it would be inefficient computationally to use Eq. (13) for states exhibiting such an order.

D. Universality of the total one-body correlations

For a system with an arbitrary number of flavors N, and an arbitrary configuration of the spins obeying the condition in Eq. (3), it is of interest to determine the total one-body correlation function (the sum over all spin flavors)

$$C_l(x) = \sum_{\sigma=1}^{N} C_l^{\sigma}(x)\,. \tag{14}$$

This can be done combining Eqs. (13) and (14), so that the sum over distinct spin flavors is replaced by the sum over all particles, $C_l(x) = \sum_{\sigma_j=1}^{N_p} C_l^{\sigma_j}(x)$. It yields

$$\begin{aligned} C_l(x) =& \frac{1}{N_p}\sum_{k=0}^{N_p-1}\sum_{\sigma_j=1}^{N_p} e^{-\frac{2\pi i}{N_p}\sigma_j k} \\ & \times \langle \hat{c}^{\dagger}_{l+x}\hat{c}_l\,\hat{\mathcal{M}}_{l,x}\exp\left[\frac{2\pi i}{N_p}k\sum_{j=1}^{l}\hat{c}^{\dagger}_j\hat{c}_j\right]\rangle \\ =& \sum_{k=0}^{N_p-1}\delta_{k,0}\langle \hat{c}^{\dagger}_{l+x}\hat{c}_l\,\hat{\mathcal{M}}_{l,x}\exp\left[\frac{2\pi i}{N_p}k\sum_{j=1}^{l}\hat{c}^{\dagger}_j\hat{c}_j\right]\rangle \\ =& \langle \hat{c}^{\dagger}_{l+x}\hat{c}_l\,\hat{\mathcal{M}}_{l,x}\rangle\,. \end{aligned} \tag{15}$$

Equation (15) shows that the total one-body correlations are independent of the number of flavors and of the particular spin pattern selected, so long as the condition in Eq. (3) is satisfied. Only the projector $\hat{\mathcal{M}}_{l,x}$ is needed when computing $C_l(x)$. The result in Eq. (15) is one of our motivations for calling the impenetrable SU(N) model under the constraints imposed to the spin configurations a model for DQPs.

III. GROUND STATE

We now turn our attention to the DQP model with spin configurations that exhibit generalized Neel order, Eq. (4). Here we study ground state properties. In Sec. IV, we study finite temperature properties.

A. Numerical implementation

We use a numerical procedure based on properties of Slater determinants to calculate one-body correlation functions (analogous to the one introduced in Refs. [49, 50] for hard-core bosons). We express Eq. (6) as

$$C_l^{\sigma}(x) = \delta_{x,0}\langle\Psi^G_{\rm SF}|\hat{\mathcal{P}}^{(\sigma)}_{l,x}|\Psi^G_{\rm SF}\rangle - \langle\Psi^G_{\rm SF}|\hat{c}_l\hat{c}^{\dagger}_{l+x}\hat{\mathcal{P}}^{(\sigma)}_{l,x}|\Psi^G_{\rm SF}\rangle\,, \tag{16}$$

where the ground state for spinless fermions is a Slater determinant, which can be written as $|\Psi^G_{\rm SF}\rangle = \prod_{j=1}^{N_p}\sum_{m=1}^{L} G_{mj}\hat{c}^{\dagger}_m|\emptyset\rangle$. The projection operator defined in Eqs. (7)-(9) changes the spinless fermion ground state into the linear combination of Slater determinants

$$\hat{\mathcal{P}}^{(\sigma)}_{l,x}|\Psi^G_{\rm SF}\rangle = \frac{1}{N}\sum_{k=0}^{N-1} e^{-\frac{2\pi i}{N}\sigma k}\prod_{j=1}^{N_p}\sum_{m=1}^{L} G^k_{mj}\hat{c}^{\dagger}_m|\emptyset\rangle\,, \tag{17}$$

with

$$G^k_{mj} = \begin{cases} e^{\frac{2\pi i}{N}k}G_{mj} & m \le l \\ 0 & l < m < l+x \\ G_{mj} & \text{otherwise} \end{cases}\,. \tag{18}$$

The modifications in G^k_{mj} with respect to G_{mj} are due to $\hat{\mathcal{R}}^{(\sigma)}_l(N)$ for $m \le l$, and due to $\hat{\mathcal{M}}_{l,x}$ for $l < m < l+x$. Next, we use that $\hat{c}^{\dagger}_j$ acting on a Slater determinant, specified by a matrix $\mathbf{G}$ with N_p columns, results in a new Slater determinant specified by a matrix $\mathbf{G}'$ that is just $\mathbf{G}$ with an added column $G'_{m,N_p+1} = \delta_{m,j}$. This means that, to compute the second expectation value in Eq. (16), we need to change $\mathbf{G} \to \mathbf{G}'$ when acting with $\hat{c}_l$ on the left, and $\mathbf{G}^k \to \mathbf{G}'^k$ when acting with $\hat{c}^{\dagger}_{l+x}$ on the right. (Here, $\mathbf{G}$ and $\mathbf{G}^k$ are matrices with elements G_{ij} and G^k_{ij}, respectively.) The final step to evaluate Eq. (16) is to compute the inner product of Slater determinants, which is equal to the determinant of the product of the matrices specifying the Slater determinants [49, 50].

Putting all the above together, the one-body correlation function can be calculated as

$$C_l^{\sigma}(x) = \frac{1}{N}\sum_{k=0}^{N-1} e^{-\frac{2\pi i}{N}\sigma k}(\delta_{x,0}\det[\mathbf{G}^{\dagger}\mathbf{G}^k] - \det[\mathbf{G}'^{\dagger}\mathbf{G}'^k])\,. \tag{19}$$

The total one-body correlation function $C_l(x)$ is much simpler to calculate, following the procedure outlined above we get:

$$C_l(x) = \delta_{x,0}\det[\mathbf{G}^{\dagger}\mathbf{G}^{k=0}] - \det[\mathbf{G}'^{\dagger}\mathbf{G}'^{k=0}]\,. \tag{20}$$

B. Results for finite systems

In Fig. 2, we plot the site occupations $n_l^{\sigma} \equiv C_l^{\sigma}(0)$ of different spin flavors in the ground state of $N_p = 12$ impenetrable fermions with a generalized Neel pattern in a lattice with $L = 240$ sites. We show results for the SU(2), SU(3), SU(4) and SU(N_p) cases in panels (a)–(d), respectively. Note that, in those finite systems at low filling, particles have relatively well defined regions of the lattice in which they can be found. Figure 2 also shows

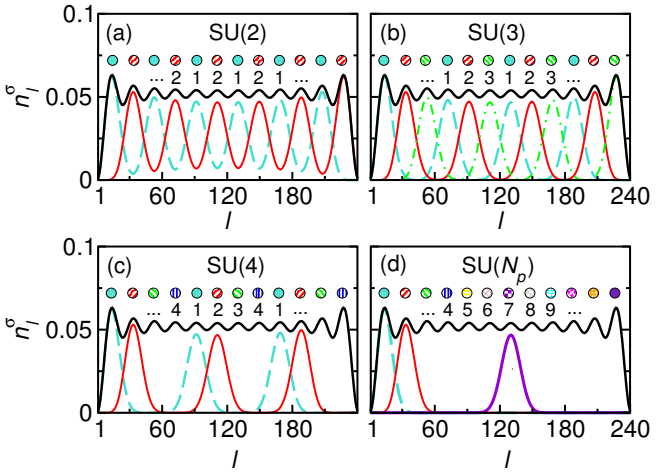

FIG. 2. Site occupations n_l^σ in the ground state of the (a) SU(2), (b) SU(3), (c) SU(4), and (d) SU(N_p) models, for $N_p = 12$ particles in an open chain with $L = 240$ sites. The spheres highlight the spin flavors, with the numbers below them indicating the corresponding value of σ. In (c) and (d) we only show n_l^σ for a few spin flavors. The thick solid line on top of the n_l^σ profiles shows the total (the sum over all spin flavors) site occupations, which are identical to the ones of the corresponding spinless fermion Hamiltonian, Eq. (5).

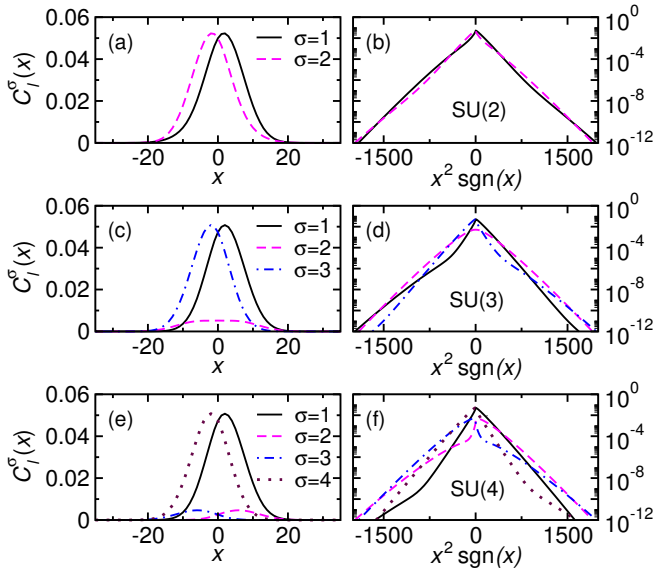

FIG. 3. One-body correlations $C_l^\sigma(x)$ in the ground state of the [(a),(b)] SU(2), [(c),(d)] SU(3), and [(e),(f)] SU(4) models. The results are for open chains with $L = 2401$ sites, a total number of particles $N_p = 240$, and for $l = 1201$ (the site at the center of the chain). The results in panels (b), (d), and (f) are the same as in panels (a), (c) and (e), respectively. The only difference is that the axes are rescaled.

the total (the sum over all spin flavors) site occupations $n_l = \sum_\sigma n_l^\sigma$ (black solid lines on top of the spin-resolved site occupations). They are identical to the site occupations in the model of spinless fermions [Eq. (5)] onto which each constrained SU(N) model is mapped. In finite systems, small peaks in n_l are the remnants of the DQP positions. What happens in the thermodynamic limit for systems in which N is $O(1)$, namely, when N does not scale with N_p, will be discussed in Sec. III C.

The left panels in Fig. 3 show the behavior (in a linear scale) of the off-diagonal matrix elements of the one-body correlation matrix $C_l^\sigma(x)$, with l being the site at the center of an open chain with $L = 2401$. Results for $C_l^\sigma(x)$ are shown for all spin flavors in the SU(2), SU(3), and SU(4) models. $C_l^\sigma(x)$ can be seen to depend on σ, which is consistent with the observation in Fig. 2 that, in finite systems, particles (and hence flavors) can be found in relatively well defined regions of the lattice.

The right panels in Fig. 3 show the same $C_l^\sigma(x)$ as in the left panels but plotted in a log scale versus $x^2\mathrm{sgn}(x)$. Most of the curves exhibit a near-linear decay with x^2, which indicates a near Gaussian decay of one-body correlations. In Sec. III D, we show that the total one-body correlations $C_l(x)$ exhibit a Gaussian decay in finite systems (even smaller than the ones in Fig. 3). In Sec. III C, we will argue that $C_l^\sigma(x)$ exhibits a Gaussian decay in the thermodynamic limit in systems in which N is $O(1)$.

An observable that is of special interest to experiments with ultracold gases in optical lattices is the quasimomentum distribution function

$$m_k^\sigma = \frac{1}{L}\sum_{l,x} e^{-ikx} C_l^\sigma(x)\,, \tag{21}$$

which can be measured using time-of-flight or band-mapping techniques [14].

In Fig. 4, we plot m_k^σ for all flavors in open chains with 1200 sites. In Fig. 4(a), we show results for the SU(3) case in systems at filling $n = N_p/L = 0.1$, while in Fig. 4(b) we show results for the SU(6) case at filling $n = 0.5$. A remarkable property of m_k^σ when compared to n_l^σ is that, in finite systems, the former is almost identical for all flavors despite the fact that the latter is not. The average carried by the sums in Eq. (21) somehow erases the differences seen in $C_l^\sigma(x)$ for each σ and l.

The dashed lines in Figs. 4(a) and 4(b) show the result for the average m_k^σ over all spin flavors, $\overline{m}_k = \sum_\sigma m_k^\sigma/N = m_k/N$. As expected, the average follows the results for each value of σ. What is more interesting is to quantify how the differences between the curves for different flavors and the average change when one changes the system size. To do that, we compute the average deviation D

$$D = \sum_{\sigma=1}^{N} D^\sigma\,, \quad \text{where} \quad D^\sigma = \frac{1}{2N_p}\sum_k |m_k^\sigma - \overline{m}_k|\,. \tag{22}$$

The maximal possible value of D is 1.

In the insets of Figs. 4(a) and 4(b), we plot D versus L for chains with the same filling n and number of flavors

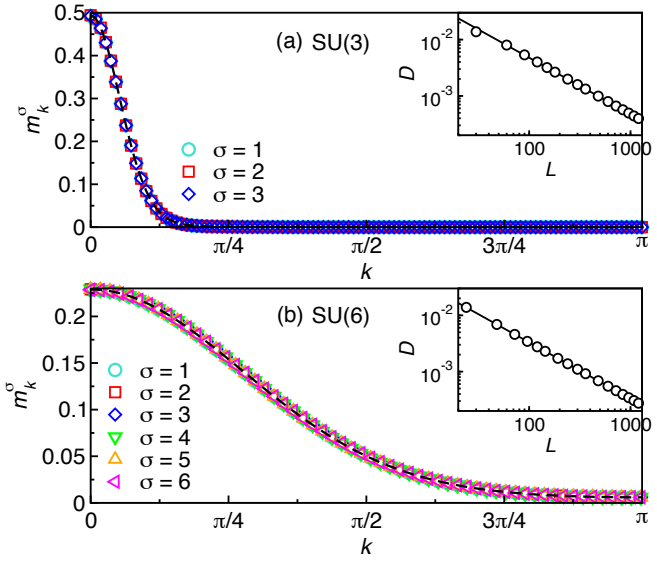

FIG. 4. Quasimomentum distribution function m_k^σ in the ground state of: (a) the SU(3) model at filling $n = 0.1$, and (b) the SU(6) model at filling $n = 0.5$. Dashed lines are the averaged distributions $\overline{m}_k$. The calculations were done in chains with $L = 1200$. Symbols in the insets show the corresponding average deviations D, defined in Eq. (22), plotted versus L. The solid lines are power law ($\propto L^{-\alpha}$) fits to the data, where $\alpha = 1.00$ in both insets.

N as in the main panels. Those plots show that the average deviations are small already for small chains, and decrease as a power law L^{-1}. The results in Fig. 4 make apparent that, even for small chains, one can accurately predict the quasimomentum distribution of each flavor using the total one-body correlations from Eq. (15).

C. Extrapolations to the thermodynamic limit

Given that the power-law fits in the insets of Figs. 4(a) and 4(b) suggest that m_k^σ becomes independent of σ in the thermodynamic limit, here we study what happens to the one-body correlation matrix when one increases the system size. We focus on the case in which N is $O(1)$, for which there is a well defined filling per flavor $n^\sigma = N_p/(NL)$ in the thermodynamic limit. In our calculations we take $N \ll N_p$, for which robust finite-size scalings can be obtained.

Let us first address what happens to the site occupations n_l^σ, shown in Fig. 2 for a finite chain, as one increases the chain size. For spinless fermions one knows that, in the thermodynamic limit away from the boundaries (after the Friedel oscillations have died out), the site occupations are position independent equal to $n = N_p/L$.

In Fig. 5(a), we show $n_l^{\sigma=1}$ about the center of chains with three sizes, for the SU(2) model at a filling $n = 0.1$. The differences between the maxima and the minima of $n_l^{\sigma=1}$ can be seen to decrease with increasing system size. To quantify them, we compute the difference of the site

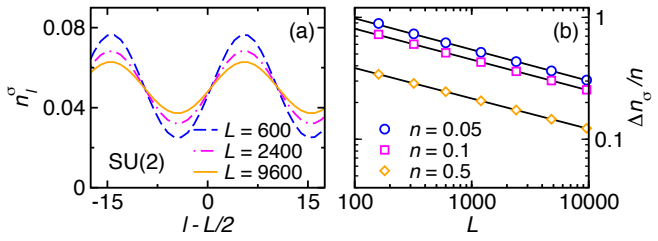

FIG. 5. (a) Ground-state site occupations n_l^σ (for $\sigma = 1$) in the SU(2) model at filling $n = 0.1$, about the center of chains with different sizes. (b) Normalized difference $\Delta n_\sigma/n$ (for $\sigma = 1$) between the site occupation at the peak and the dip closest to the chain center, for different fillings $n = 0.05$, 0.1 and 0.5. Solid lines are power law fits $\Delta n_\sigma/n \propto L^{-\alpha}$ with $\alpha \simeq 0.25$.

occupation at the peak $n_{l_{\rm peak}}^\sigma$ and at the dip $n_{l_{\rm dip}}^\sigma$ that are closest to the lattice center, $\Delta n_\sigma = n_{l_{\rm peak}}^\sigma - n_{l_{\rm dip}}^\sigma$. Results for $\Delta n_{\sigma=1}/n$ for the SU(2) model at three different values of n are plotted in Fig. 5(b) versus L. All three can be seen to decrease as power laws $\propto L^{-\alpha}$ with $\alpha \simeq 0.25$. This suggest that, with increasing system size, the site occupations n_l^σ become position independent away from the edges of the chain (as for spinless fermions), and are equal to n^σ. This means that the structures seen in n_l^σ in Fig. 2, which could be observed in experiments with ultracold fermions in optical lattices (in which $L \sim 100$), disappear in the thermodynamic limit away from the edges of the chain.

The results for m_k^σ and n_l^σ with increasing system size suggest that the one-body correlation matrices $\mathbf{C}^\sigma$ approach the average (over all flavors) one-body correlation matrix $\overline{\mathbf{C}} = \sum_{\sigma=1}^N \mathbf{C}^\sigma/N$ away from the edges of the chain. To verify this, we calculate the trace distances

$$d[\mathbf{C}^\sigma, \overline{\mathbf{C}}] = \frac{1}{2N_p} \mathrm{Tr} \left\{ \sqrt{[\mathbf{C}^\sigma - \overline{\mathbf{C}}]^2} \right\} , \qquad (23)$$

for all flavors. Figures 6(a) and 6(b) show $\sum_{\sigma=1}^N d[\mathbf{C}^\sigma, \overline{\mathbf{C}}]$ versus L for the SU(2) and SU(3) models, respectively, at

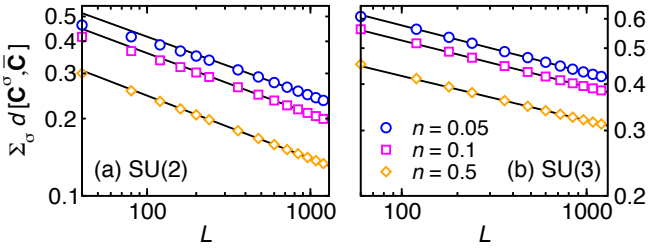

FIG. 6. Sums over trace distances $\sum_\sigma d[\mathbf{C}^\sigma, \overline{\mathbf{C}}]$ of the $\mathbf{C}^\sigma$ and $\overline{\mathbf{C}}$ one-body correlation matrices, where $d[\mathbf{C}^\sigma, \overline{\mathbf{C}}]$ is defined in Eq. (23). Results are shown for different fillings n in the ground state of the (a) SU(2) and (b) SU(3) model. In all the cases the sums decrease as power laws. This is made apparent by the fits $\propto L^{-\alpha}$ depicted as solid lines, with $\alpha \simeq 0.25$ in (a) and $\alpha \simeq 0.12$ in (b).

different fillings. With increasing system size, one can see that the added trace distances decrease as power laws in L. This suggests that the one-body correlation matrices $\mathbf{C}^\sigma$ are, up to nonextensive deviations (due to boundary effects), identical for all σ in the thermodynamic limit.

However, it is important to stress that, in contrast to the results for m_k^σ reported in Fig. 4, the results for n_l^σ in Fig. 5 and for $\sum_{\sigma=1}^{N} d[\mathbf{C}^\sigma, \overline{\mathbf{C}}]$ in Fig. 6 reveal that the spin-resolved one-body correlation functions can be quite different from the average in finite systems. These differences are likely not negligible for the system sizes relevant to ultracold atom experiments. Moreover, the differences from the average increase with increasing the number of flavors N.

D. Total one-body correlations

Since in the previous section we argued that the total one-body correlations $C_l(x)$ [divided by N, with N being $O(1)$] become identical to the flavor resolved ones $C_l^\sigma(x)$ in thermodynamic limit, in what follows we focus our study on $C_l(x)$. The total one-body correlations $C_l(x)$ were introduced in Eqs. (14)-(15) as an observable that highlights a universal property of the DQP model. In such a model, $C_l(x)$ neither depends on the number of flavors nor on the specific spin configuration (with contiguous fermions having distinct spin flavors). If one is interested in describing experiments, $C_l(x)$ may be good enough to describe quasimomentum distribution functions, but a calculation of $C_l^\sigma(x)$ may be needed to obtain accurate results for the spin resolved site occupation profiles in small chains.

In Fig. 7(a), we show the decay of $C_l(x)$ measured from different sites l, in a chain with $L = 1200$ sites at filling $n = 0.5$. The overlap between the results for different values of l is nearly perfect, and the decay of $C_l(x)$ with x is clearly Gaussian

$$C_l(x) = n\, e^{-x^2/x_0^2}\,, \tag{24}$$

where x_0 is the width. Equation (24) is a defining property of the DQP model, and it is one of the main results of this work.

The Gaussian decay of the total one-body correlations $C_l(x)$ is a robust property of the DQP model. The robustness is characterized by three properties. First, as mentioned before, Fig. 7(a) shows that $C_l(x)$ measured from different sites l yields nearly identical results even if l is close to the boundaries of a finite chain. Second, Fig. 7(b) shows that $C_l(x)$ is Gaussian for different chain fillings n. And third, Fig. 12 in Appendix A shows that $C_l(x)$ is independent of the system size L for $L \gtrsim 100$.

A key property of our setup, which we expect gives rise to the Gaussian decay of $C_l(x)$, is the distinguishability of the quantum particles [enforced by the projector $\hat{\mathcal{M}}_{l,x}$ defined in Eq. (8)]. Such a Gaussian decay is fundamentally different from the known power-law decay of

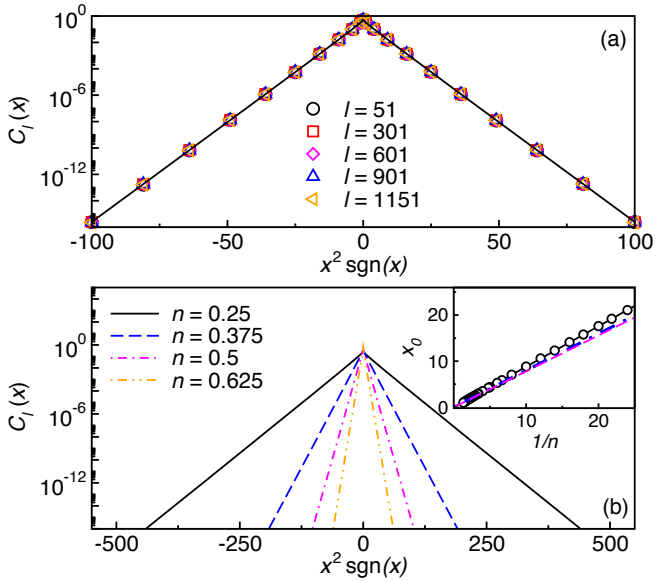

FIG. 7. Total one-body correlation function $C_l(x)$ in the ground state of a chain with $L = 1200$. (a) $C_l(x)$ versus x at filling $n = 0.5$ for different values of l. There is data collapse for all values of l shown. (b) $C_l(x)$ measured from the center of the lattice, $l = L/2 + 1$, for different fillings n. In all cases $C_l(x)$ can be seen to be Gaussian. In the inset of (b), the symbols depict the width x_0 of the Gaussian decay versus $1/n$. x_0 was obtained by fitting $C_l(x)$ to Eq. (24). The solid line is a linear fit to the data with slope 0.88, while the dashed and dotted lines are $x_0^{(\mathrm{SF})}$ from Eq. (26), and $x_0^{(\mathrm{HO})}$ from Eq. (27), respectively.

one-body correlations of spinless fermions

$$\langle \hat{c}_{l+x}^\dagger \hat{c}_l \rangle = \frac{\sin(nx\pi)}{x\pi}\,. \tag{25}$$

It remains to be understood how the width x_0 of the Gaussian decay, Eq. (24), depends on the chain's filling. Dimensional analysis suggests that it is proportional to the average distance between particles, $x_0 \propto n^{-1}$. The proportionality constant can be estimated by assuming that the correlations in the DQP model and in the spinless fermion model approach each other when $nx \to 0$, i.e., at short distances when particle exchange ceases to play a role. Matching the second term in the expansion of Eqs. (24) and (25) about $x = 0$ yields

$$x_0^{(\mathrm{SF})} = \frac{1}{n}\frac{\sqrt{6}}{\pi}\,. \tag{26}$$

We compare $x_0^{(\mathrm{SF})}$ with the values of x_0 obtained by fitting $C_l(x)$ with the Gaussian function in Eq. (24). The results, shown in the inset of Fig. 7(b), make apparent that x_0 is reasonable close to $x_0^{(\mathrm{SF})}$.

Interestingly, the ground state correlations of a single particle in a harmonic oscillator are also Gaussian. The ground state wavefunction of such a system has the form $u_0(x) = \sqrt{n}e^{-(nx)^2\pi/2}$, where n is the density at the

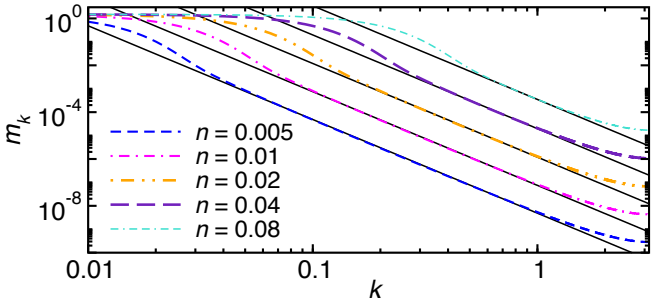

FIG. 8. High-momentum tails of the quasimomentum distribution m_k of DQPs at low fillings in chains with $L = 5000$ sites. Solid lines show fits to the expected $1/k^4$ behavior, which shrinks (and eventually disappears) with increasing filling as all momenta in the Brillouin zone become increasingly populated.

center of the trap (related to the mass m and the trap frequency ω by $n^2\pi = m\omega/\hbar$). The correlation function $u_0(0)u_0(x)$ exhibits a Gaussian decay with a width

$$x_0^{(\mathrm{HO})} = \frac{1}{n}\frac{\sqrt{2\pi}}{\pi}. \tag{27}$$

$x_0^{(\mathrm{HO})}$, which is also plotted in the inset of Fig. 7(b), is very close to $x_0^{(\mathrm{SF})}$ and is also close to x_0.

Finally, related to the short distance correlations of DQPs, it is important to note that, at low fillings, the quasimomentum distribution function m_k of DQPs exhibits the $1/k^4$ tail that is known to appear in other models with contact interactions [13]. In Fig. 8, we plot m_k vs k in chains at low fillings. Fits to $1/k^4$ decay, depicted as solid lines, make apparent the region in k in which the corresponding $1/k^4$ behavior occurs in m_k. Note that, with increasing filling, m_k increases over the entire Brillouin zone and the region in which $1/k^4$ behavior occurs shrinks. It eventually disappears as all quasimomentum modes become significantly populated. Indications of such $1/k^4$ tails in impenetrable SU(N) fermions in the continuum were recently reported in Ref. [33]. As for hard-core boson systems [49, 51], our numerical approach in the lattice allows one to resolve those tails better than approaches that work directly in the continuum.

IV. FINITE TEMPERATURE

We now turn our attention to finite temperature properties of the DQP model. We focus on the temperature dependence of the total one-body correlations $C_l(x;T)$. The total one-body correlations were shown in Sec. III to be universal, and to characterise flavor resolved one-body correlations in the thermodynamic limit when N is $O(1)$.

A. Numerical implementation

In order to compute the finite-temperature correlations of the DQP model, we develop a computational procedure similar to the one introduced for hard-core bosons in Ref. [52].

The two basic relations needed to make the finite-temperature calculations in polynomial time are [52]: (i) Traces over the fermionic Fock space of exponentials that are bilinear in fermionic creation and annihilation operators satisfy

$$\mathrm{Tr}\left[\exp\left(\sum_{ij}\hat{c}_i^\dagger X_{ij}\hat{c}_j\right)\exp\left(\sum_{kl}\hat{c}_k^\dagger Y_{kl}\hat{c}_l\right)\ldots\right] = \det\left[\mathbf{I}+e^{\mathbf{X}}e^{\mathbf{Y}}\ldots\right]. \tag{28}$$

(ii) The one-body operator $\hat{c}_l^\dagger\hat{c}_j$, for $l \neq j$, can be written as

$$\hat{c}_l^\dagger\hat{c}_j = \exp\left(\sum_{mn}\hat{c}_m^\dagger A_{mn}\hat{c}_n\right) - 1, \tag{29}$$

where the only nonzero element of $\mathbf{A}$ is $A_{lj} = 1$.

Using those two relations, one can write the total one-body correlation at finite temperature $C_l(x;T)$ as

$$C_l(x\neq 0;T) = \frac{1}{Z}\{\det[\mathbf{I}+(\mathbf{I}+\mathbf{A})\mathbf{M}_{l,x}\mathbf{U}e^{-(\mathbf{E}-\mu\mathbf{I})/T}\mathbf{U}^\dagger] - \det[\mathbf{I}+\mathbf{M}_{l,x}\mathbf{U}e^{-(\mathbf{E}-\mu\mathbf{I})/T}\mathbf{U}^\dagger]\}, \tag{30}$$

where, $\mathbf{I}$ is the identity matrix, $\mathbf{A}$ is a matrix in which the only non-zero element is $A_{l,l+x} = 1$ [from Eq. (29)], $\mathbf{U}$ is the unitary matrix that diagonalizes the corresponding spinless fermion Hamiltonian $\hat{H}_{\mathrm{SF}}$ in Eq. (5), $\mathbf{H}_{\mathrm{SF}} = \mathbf{U}\mathbf{E}\mathbf{U}^\dagger$, with $\mathbf{E}$ being the diagonal matrix that contains all the single-particle eigenenergies, $Z = \prod_i[1+e^{-(E_{ii}-\mu)/T}]$ is the partition function, and $\mathbf{M}_{l,x}$ is the matrix representation of the projection operator $\hat{\mathcal{M}}_{l,x}$, see Eq. (8), which is a diagonal matrix with elements 0 between $l+1$ and $l+x-1$, and 1 otherwise.

The diagonal matrix elements of $C_l(x;T)$ are the same as for spinless fermions

$$C_l(0;T) = 1 - [\mathbf{I}+e^{-(\mathbf{H}_{\mathrm{SF}}-\mu\mathbf{I})/T}]^{-1}_{ii}, \tag{31}$$

and the chemical potential μ is determined so that the total number of particles is $N_p = \sum_l C_l(0;T)$.

B. Total one-body correlations

In Fig. 9(a) we plot the total one-body correlation function $C_l(x;T)$ versus x^2 for various temperatures. Figure 9(a) shows that $\log C_l(x;T)$ becomes a convex function of x^2 at $T > 0$, which indicates that its decay is $\propto x^{\gamma(T)}$, with $\gamma(T) < 2$. To describe the decay at finite temperatures, we use the following fitting ansatz

$$C_l(x;T) = n\,\exp\{-[x/x_0(T)]^{\gamma(T)}\}, \tag{32}$$

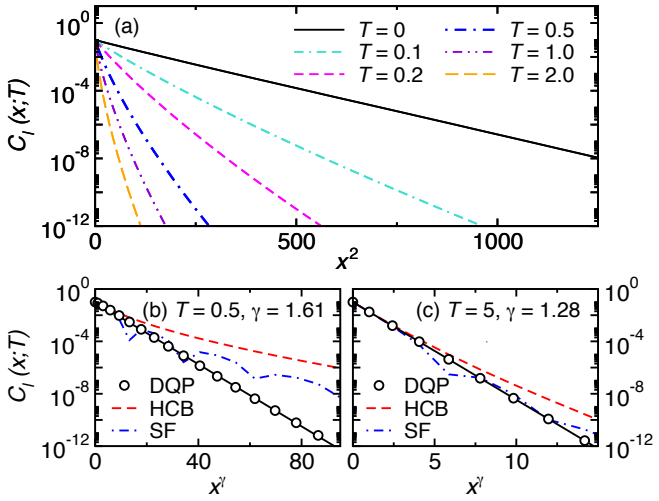

FIG. 9. Total one-body correlation function $C_l(x;T)$ at finite temperature in chains with $L = 1200$, $l = L/2 + 1$, at filling $n = 0.05$. (a) $C_l(x;T)$ in the DQP model as a function of x^2, for six different temperatures. (b) and (c) Results for $T = 0.5$ and 5, respectively, plotted as functions of $x^{\gamma(T)}$, where $\gamma(T)$ is the exponent extracted by fitting $C_l(x;T)$ with the ansatz in Eq. (32). Symbols show numerical results for the DQP model while solid lines are the corresponding fits. In (b) and (c), we compare the results obtained for the DQP model with those for the absolute value of the one-body correlations of spinless fermions (SF, dashed dotted line) to which the DQP model is mapped. Results are also shown for hard-core bosons (HCB, dashed line), which can also be mapped onto the same spinless fermion Hamiltonian [13].

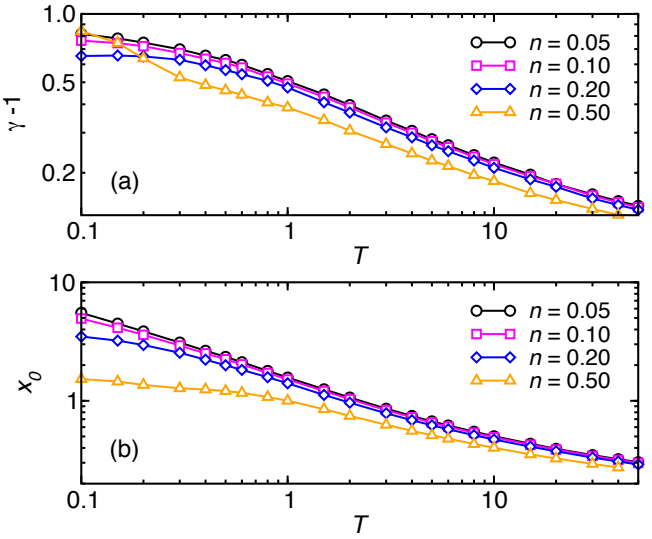

FIG. 10. (a) $\gamma(T)$ and (b) $x_0(T)$, obtained by fitting our numerical results with Eq. (32), plotted as functions of T for different fillings n. The symbols show the numerical results, while the solid lines are guides to the eye.

for which we determine the exponent $\gamma(T)$, and the effective width $x_0(T)$, as functions of the temperature. We fit $\log C_l(x;T)$ from $x = 0$ through all the sites in which $C_l(x;T) \geq 10^{-12}$, and choose temperatures such that the fitting includes at least six points. The latter constrains the highest temperatures for which we do fits.

Examples of fits using Eq. (32) are reported in Figs. 9(b) and 9(c) for temperatures $T = 0.5$ and 5, respectively, in systems with $n = 0.1$. (The numerical results for $C_l(x;T)$ are shown as symbols and the fits are shown as solid lines.) Note the near perfect overlap between the numerical results and the fits, as well as the fact that $\log C_l(x;T)$ versus $x^{\gamma(T)}$ exhibits a linear decrease when the appropriate value of $\gamma(T)$ is used, i.e., those plots make apparent that the ansatz in Eq. (32) provides an accurate description of the total one-body correlations at finite temperature.

The values of $\gamma(T)$ obtained in Figs. 9(b) and 9(c) suggest that $\log C_l(x;T)$ approaches a linear function of x as T increases. This is consistent with the intuition that, at very high temperature, the statistics of the particles ceases to play a role and one-body correlations of impenetrable SU(N) fermions should become identical to those of the spinless fermions to which they are mapped, for which an exponential decay is known to occur at finite temperature. In Figs. 9(b) and 9(c), we also show the one-body correlations for the corresponding spinless fermions and hard-core bosons (see Appendix B for the definition of hard-core bosons). Hard-core bosons are also mappable to the spinless fermion Hamiltonian to which we mapped the constrained impenetrable SU(N) fermions [13]. As expected, the results for all three models approach each other with increasing temperature.

Figure 10(a) shows how $\gamma(T)$ approaches 1 with increasing temperature for different fillings n. It is interesting to note that, despite the fact that the exponent of the stretched exponential decreases with increasing temperature, Fig. 9(a) shows that the higher the temperature the smaller the correlations at any given distance x, for $C_l(x;T) \geq 10^{-12}$. This occurs because, as shown in Fig. 10(b), $x_0(T)$ also decreases with increasing temperature. We should add that the departure of $C_l(x;T)$ from a Gaussian at finite temperature results in an enhancement of one-body correlations at long distances with respect to the ground state (see Appendix C) This is something that may be of experimental interest at low temperatures.

To conclude, we report results for the total quasimomentum distribution function $m_k(T) = \sum_{l,x} e^{ikx} C_l(x;T)/L$, which is of special interest to experiments with ultracold fermions. $m_k(T)$ for the DQP model is shown in Fig. 11 at three different temperatures $T = 0$, 0.5, and 5. In that figure, we also show the quasimomentum distribution functions of spinless fermions and hard-core bosons at the same temperatures.

In the ground state, m_k of DQPs shows a smooth peak near $k = 0$ (see also Fig. 4). This is in stark contrast to the quasimomentum distribution of spinless fermions, which exhibits a step like distribution with a Fermi edge,

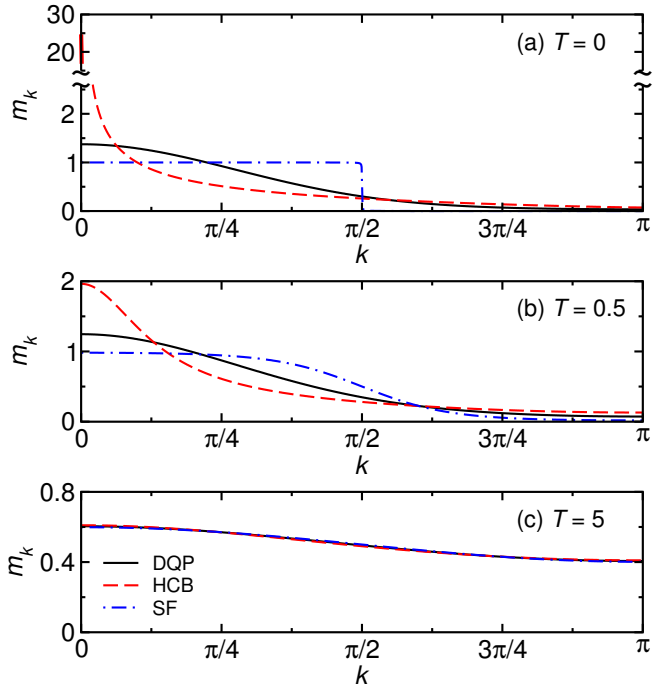

FIG. 11. Quasimomentum distribution function m_k of DQPs (DQP, solid lines), spinless fermions (SF, dashed-dotted lines), and hard-core bosons (HCB, dashed lines) at (a) $T = 0$, (b) $T = 0.5$, and (c) $T = 5$. The results were obtained in chains with $L = 1200$ sites at filling $n = 0.5$.

and of hard-core bosons, which exhibits a sharp peak at $k = 0$ (note the discontinuity in the y-axis) making apparent the occurrence of quasicondensation [13, 49, 50]. Temperatures below the energy scale of the hopping [see Fig. 11(b)] do not change much the quasimomentum distribution of DQPs, change the quasimomentum distribution of spinless fermions about the Fermi edge, and have a dramatic effect in the quasimomentum distribution of hard-core bosons. The latter occurs because one-body correlations switch from power-law to exponentially decaying when T becomes nonzero [52]. At temperatures above the bandwidth of the spinless fermions model (4 in our units), see Fig. 11(c), the quasimomentum distribution of DQPs, spinless fermions, and hard-core bosons become near indistinguishable. This, which is consistent with the results for $C_l(x;T)$ shown in Fig. 9(c), highlights the irrelevance of the particle statistics in m_k at those temperatures.

V. SUMMARY

We have studied impenetrable SU(N) fermions within sectors of the Hamiltonian in which consecutive fermions have different spin flavors. We call this constrained model a model of distinguishable quantum particles (DQPs), for which the original statistics of the particles plays no role. This is because contiguous particles have different spin flavors and particle exchanges are forbidden by the impenetrability constraint. Consequently, our results apply equally to impenetrable SU(N) bosons under the same constraint that contiguous bosons have different spin flavors. For the model of DQPs, we introduced an exact numerical approach based on a mapping onto noninteracting spinless fermions that allows one to compute spin resolved one-body correlation functions in eigenstates of the Hamiltonian and at finite temperature.

We showed that, in the ground state of the DQP model, the decay of one-body correlations is Gaussian. This is in contrast to the power-law or exponential decay known to occur in the ground state of traditional 1D models [13]. We also showed that, at low fillings in the lattice, the quasimomentum distribution function of DQPs exhibits a $1/k^4$ tail. At finite temperature, we showed that one-body correlations are well described by a stretched exponential decay, with an exponent that transitions between 2 and 1 as the temperature increases. Namely, the correlations transition between Gaussian in the ground state and exponential at high temperature. At high temperatures, we also showed that the momentum distribution function of DQPs becomes identical to those of spinless fermions and hard-core bosons.

As an outlook, it would be interesting to find other models in 1D in which one-body correlations exhibit a Gaussian decay in the ground state. This might help shed further light on the conditions needed for such correlations to occur and on the universality of our results.

VI. ACKNOWLEDGMENTS

We acknowledge discussions with T. Čadež, M. Endres, P. Prelovšek, and T. Prosen. Y.Z. and M.R. acknowledge support by the NSF Grant No. PHY-1707482. Y.Z. acknowledges support by Advanced grant of European Research Council (ERC) 694544-OMNES. L.V. acknowledges support from the Slovenian Research Agency (research core funding No. P1-0044).

Appendix A: Finite size effects of $C_l(x)$ in the ground state

In Fig. 12, we show $C_l(x)$ for five chains of different sizes L at filling $n = 0.5$. The results for $C_l(x)$ agree with each other independently of the values of L chosen, which means that finite-size effects for the total one-body correlations are negligible already for systems with $L \sim 100$. This is in stark contrast to the spin resolved correlations $C_l^\sigma(x)$, see Fig. 6, which can exhibit significant finite size effects for much larger chain sizes.

In Fig. 7, we chose $L = 1200$ for the calculations of $C_l(x)$. For such a chain size, we expect the numerical results to be indistinguishable from those in the thermodynamic limit.

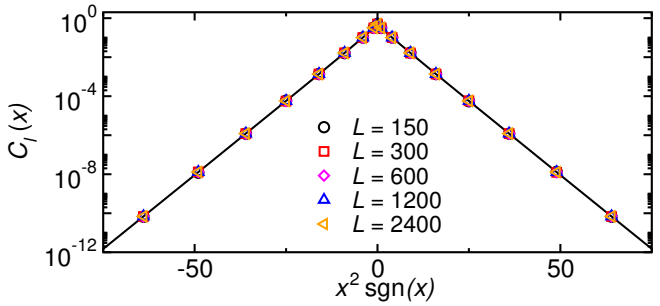

FIG. 12. Total one-body correlation function $C_l(x)$ in the ground state of five chains of different sizes. The filling is fixed to $n = 0.5$, and l is chosen to be $l = L/2+1$. The results for different chain sizes L are virtually indistinguishable.

Appendix B: Hard-core bosons

The hard-core boson Hamiltonian can be written as

$$\hat{H}_{\rm HCB} = -\sum_{l=1}^{L-1} \left(\hat{b}_{l+1}^\dagger \hat{b}_l + {\rm H.c.} \right) , \qquad \text{(B1)}$$

supplemented by the constraints $(\hat{b}_l)^2 = (\hat{b}_l^\dagger)^2 = 0$, where $\hat{b}_l^\dagger$ ($\hat{b}_l$) is the creation (annihilation) operator of a hard-core boson at site l. This model is the infinite on-site repulsion limit of the Bose-Hubbard model [13]. By virtue of the Holstein-Primakoff and the Jordan-Wigner transformations [13, 53, 54], one can map the Hamiltonian in Eq. (B1) onto a Hamiltonian of spinless fermions, Eq. (5), using $\hat{b}_l = e^{i\pi \sum_{m<l} \hat{c}_m^\dagger \hat{c}_m} \hat{c}_l$. We calculate the one-body correlations of hard-core bosons using the approach introduced in Refs. [49, 50] for the ground state, and in Ref. [52] for finite temperature.

Appendix C: Low temperature behavior of $C_l(x;T)$

Figure 13 shows the low and intermediate temperature behavior of $C_l(x;T)$ versus x at filling $n = 0.5$. The main point to be highlighted about those results is that while finite temperatures always reduce the total one-body correlations at short distances, the switch from Gaussian in the ground state to stretched exponential decay at finite temperature (see the inset) results in an enhancement of the total one-body correlations at long distances. This enhancement is likely to be relevant to experiments only at low temperatures, so that the correlations are not too small to be detected. Such a finite-temperature behavior at long distances, not apparent in the occupations of the low-k momenta which decrease with increasing temperature [see Figs. 11(a) and 11(b)], is another remarkable property of DQPs when compared to traditional one-dimensional models. In the latter models, one-body correlations at long distances are usually reduced at finite temperatures with respect to the ground state.

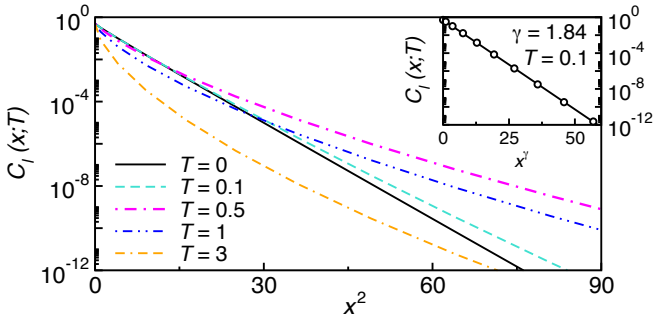

FIG. 13. Total one-body correlations $C_l(x;T)$ at low and intermediate temperature for $n = 0.5$, $L = 1200$, and $l = L/2 + 1$. (Inset) Symbols depict the results for $T = 0.1$ (also shown in the main panel) while the solid line is a fit to Eq. (32) with $\gamma(T) = 1.84$.

[1] S. Tomonaga, Remarks on Bloch's Method of Sound Waves applied to Many-Fermion Problems, Progress of Theoretical Physics **5**, 544 (1950).

[2] J. M. Luttinger, An exactly soluble model of a many fermion system, J. Math. Phys. **4**, 1154 (1963).

[3] C. Kim, A. Y. Matsuura, Z.-X. Shen, N. Motoyama, H. Eisaki, S. Uchida, T. Tohyama, and S. Maekawa, Observation of spin-charge separation in one-dimensional $SrCuO_2$, Phys. Rev. Lett. **77**, 4054 (1996).

[4] P. Segovia, D. Purdie, M. Hengsberger, and Y. Baer, Observation of spin and charge collective modes in one-dimensional metallic chains, Nature **402**, 504 (1999).

[5] R. Claessen, M. Sing, U. Schwingenschlögl, P. Blaha, M. Dressel, and C. S. Jacobsen, Spectroscopic signatures of spin-charge separation in the quasi-one-dimensional organic conductor TTF-TCNQ, Phys. Rev. Lett. **88**, 096402 (2002).

[6] B. J. Kim, H. Koh, E. Rotenberg, S.-J. Oh, H. Eisaki, N. Motoyama, S. Uchida, T. Tohyama, S. Maekawa, Z.-X. Shen, and C. Kim, Distinct spinon and holon dispersions in photoemission spectral functions from one-dimensional $SrCuO_2$, Nature Phys. **2**, 397 (2006).

[7] Y. Ma, H. C. Diaz, J. Avila, C. Chen, V. Kalappattil, R. Das, M.-H. Phan, T. Čadež, J. M. P. Carmelo, M. C. Asensio, and M. Batzill, Angle resolved photoemission spectroscopy reveals spin charge separation in metallic $MoSe_2$ grain boundary, Nature Comm. **8**, 14231 (2017).

[8] M. Boll, T. A. Hilker, G. Salomon, A. Omran, J. Nespolo, L. Pollet, I. Bloch, and C. Gross, Spin- and density-resolved microscopy of antiferromagnetic correlations in Fermi-Hubbard chains, Science **353**, 1257 (2016).

[9] T. A. Hilker, G. Salomon, F. Grusdt, A. Omran, M. Boll, E. Demler, I. Bloch, and C. Gross, Revealing hidden antiferromagnetic correlations in doped hubbard chains via string correlators, Science **357**, 484 (2017).

[10] F. D. M. Haldane, 'Luttinger liquid theory' of one-dimensional quantum fluids. I. Properties of the Luttinger model and their extension to the general 1D interacting spinless Fermi gas, J. Phys. C **14**, 2585 (1981).

[11] J. Voit, One-dimensional fermi liquids, Rep. Prog. Phys. **58**, 977 (1995).

[12] T. Giamarchi, *Quantum physics in one dimension*, volume 121 of International series on monographs in physics (Oxford University Press, Oxford, 2004).

[13] M. A. Cazalilla, R. Citro, T. Giamarchi, E. Orignac, and M. Rigol, One dimensional bosons: From condensed matter systems to ultracold gases, Rev. Mod. Phys. **83**, 1405 (2011).

[14] I. Bloch, J. Dalibard, and W. Zwerger, Many-body physics with ultracold gases, Rev. Mod. Phys. **80**, 885 (2008).

[15] M. Girardeau, Relationship between systems of impenetrable bosons and fermions in one dimension, J. Math. Phys. **1**, 516 (1960).

[16] T. Kinoshita, T. Wenger, and D. S. Weiss, Observation of a one-dimensional Tonks-Girardeau gas, Science **305**, 1125 (2004).

[17] B. Paredes, A. Widera, V. Murg, O. Mandel, S. Fölling, I. Cirac, G. V. Shlyapnikov, T. W. Hänsch, and I. Bloch, Tonks-Girardeau gas of ultracold atoms in an optical lattice, Nature **429**, 277 (2004).

[18] T. Kinoshita, T. Wenger, and D. S. Weiss, Local pair correlations in one-dimensional Bose gases, Phys. Rev. Lett. **95**, 190406 (2005).

[19] C. Wu, J.-p. Hu, and S.-c. Zhang, Exact SO(5) symmetry in the spin-3/2 fermionic system, Phys. Rev. Lett. **91**, 186402 (2003).

[20] M. A. Cazalilla, A. F. Ho, and M. Ueda, Ultracold gases of ytterbium: ferromagnetism and Mott states in an SU(6) Fermi system, New J. Phys. **11**, 103033 (2009).

[21] A. V. Gorshkov, M. Hermele, V. Gurarie, C. Xu, P. S. Julienne, J. Ye, P. Zoller, E. Demler, M. D. Lukin, and A. M. Rey, Two-orbital SU(N) magnetism with ultracold alkaline-earth atoms, Nature Phys. **6**, 289 (2010).

[22] S. Taie, R. Yamazaki, S. Sugawa, and Y. Takahashi, An SU(6) Mott insulator of an atomic Fermi gas realized by large-spin Pomeranchuk cooling, Nature Phys. **8**, 825 (2012).

[23] G. Pagano, M. Mancini, G. Cappellini, P. Lombardi, F. Schäfer, H. Hu, X.-J. Liu, J. Catani, C. Sias, M. Inguscio, and L. Fallani, A one-dimensional liquid of fermions with tunable spin, Nature Phys. **10**, 198 (2014).

[24] F. Scazza, C. Hofrichter, M. Höfer, P. C. D. Groot, I. Bloch, and S. Fölling, Observation of two-orbital spin-exchange interactions with ultracold SU(N)-symmetric fermions, Nature Phys. **10**, 779 (2014).

[25] X. Zhang, M. Bishof, S. L. Bromley, C. V. Kraus, M. S. Safronova, P. Zoller, A. M. Rey, and J. Ye, Spectroscopic observation of SU(N)-symmetric interactions in Sr orbital magnetism, Science **345**, 1467 (2014).

[26] M. A. Cazalilla and A. M. Rey, Ultracold fermi gases with emergent SU(N) symmetry, Rep. Prog. Phys. **77**, 124401 (2014).

[27] P. Nataf and F. Mila, Exact diagonalization of Heisenberg SU(N) models, Phys. Rev. Lett. **113**, 127204 (2014).

[28] A. G. Volosniev, D. V. Fedorov, A. S. Jensen, N. T. Zinner, and M. Valiente, Multicomponent strongly interacting few-fermion systems in one dimension, Few-Body Systems **55**, 839 (2014).

[29] J. Dufour, P. Nataf, and F. Mila, Variational Monte Carlo investigation of SU(N) Heisenberg chains, Phys. Rev. B **91**, 174427 (2015).

[30] J. Decamp, P. Armagnat, B. Fang, M. Albert, A. Minguzzi, and P. Vignolo, Exact density profiles and symmetry classification for strongly interacting multicomponent fermi gases in tight waveguides, New J. Phys. **18**, 055011 (2016).

[31] J. Decamp, J. Jünemann, M. Albert, M. Rizzi, A. Minguzzi, and P. Vignolo, High-momentum tails as magnetic-structure probes for strongly correlated SU(κ) fermionic mixtures in one-dimensional traps, Phys. Rev. A **94**, 053614 (2016).

[32] E. K. Laird, Z.-Y. Shi, M. M. Parish, and J. Levinsen, SU(N) fermions in a one-dimensional harmonic trap, Phys. Rev. A **96**, 032701 (2017).

[33] H. H. Jen and S.-K. Yip, Spin-incoherent luttinger liquid of one-dimensional su(κ) fermions, Phys. Rev. A **98**, 013623 (2018).

[34] M. Ogata and H. Shiba, Bethe-ansatz wave function, momentum distribution, and spin correlation in the one-dimensional strongly correlated Hubbard model, Phys. Rev. B **41**, 2326 (1990).

[35] A. Parola and S. Sorella, Asymptotic spin-spin correlations of the U$\to\infty$ one-dimensional Hubbard model, Phys. Rev. Lett. **64**, 1831 (1990).

[36] A. Parola and S. Sorella, Spin-charge decoupling and the Green's function of one-dimensional Mott insulators, Phys. Rev. B **45**, 13156 (1992).

[37] K. Penc, K. Hallberg, F. Mila, and H. Shiba, Shadow Band in the One-Dimensional Infinite-U Hubbard Model, Phys. Rev. Lett. **77**, 1390 (1996).

[38] K. Penc, K. Hallberg, F. Mila, and H. Shiba, Spectral functions of the one-dimensional Hubbard model in the U$\to+\infty$ limit: How to use the factorized wave function, Phys. Rev. B **55**, 15475 (1997).

[39] A. Izergin, A. Pronko, and N. Abarenkova, Temperature correlators in the one-dimensional Hubbard model in the strong coupling limit, Phys. Lett. A **245**, 537 (1998).

[40] P. Prelovšek, S. El Shawish, X. Zotos, and M. Long, Anomalous scaling of conductivity in integrable fermion systems, Phys. Rev. B **70**, 205129 (2004).

[41] B. Kumar, Canonical representation for electrons and its application to the Hubbard model, Phys. Rev. B **77**, 205115 (2008).

[42] B. Kumar, Exact solution of the infinite-U Hubbard problem and other models in one dimension, Phys. Rev. B **79**, 155121 (2009).

[43] B. Bertini, E. Tartaglia, and P. Calabrese, Quantum quench in the infinitely repulsive Hubbard model: the stationary state, J. Stat. Mech. **2017**, 103107 (2017).

[44] F. Essler, H. Frahm, F. Göhmann, A. Klümper, and V. E. Korepin, *The one-dimensional Hubbard model* (Cambridge University Press, 2005).

[45] M. Medenjak, K. Klobas, and T. Prosen, Diffusion in deterministic interacting lattice systems, Phys. Rev. Lett. **119**, 110603 (2017).
[46] S. Hild, T. Fukuhara, P. Schauß, J. Zeiher, M. Knap, E. Demler, I. Bloch, and C. Gross, Far-from-equilibrium spin transport in Heisenberg quantum magnets, Phys. Rev. Lett. **113**, 147205 (2014).
[47] E. H. Lieb and F. Y. Wu, Absence of mott transition in an exact solution of the short-range, one-band model in one dimension, Phys. Rev. Lett. **20**, 1445 (1968).
[48] H. Frahm and V. E. Korepin, Critical exponents for the one-dimensional Hubbard model, Phys. Rev. B **42**, 10553 (1990).
[49] M. Rigol and A. Muramatsu, Universal properties of hard-core bosons confined on one-dimensional lattices, Phys. Rev. A **70**, 031603 (2004).
[50] M. Rigol and A. Muramatsu, Ground-state properties of hard-core bosons confined on one-dimensional optical lattices, Phys. Rev. A **72**, 013604 (2005).
[51] W. Xu and M. Rigol, Universal scaling of density and momentum distributions in Lieb-Liniger gases, Phys. Rev. A **92**, 063623 (2015).
[52] M. Rigol, Finite-temperature properties of hard-core bosons confined on one-dimensional optical lattices, Phys. Rev. A **72**, 063607 (2005).
[53] P. Jordan and E. Wigner, Über das Paulische Äquivalenzverbot, Z. Phys. **47**, 631 (1928).
[54] T. Holstein and H. Primakoff, Field dependence of the intrinsic domain magnetization of a ferromagnet, Phys. Rev. **58**, 1098 (1940).